PNAS RESEARCH ARTICLE | NEUROSCIENCE

Distinct context- and content-dependent population codes in superior colliculus during sensation and action

Eve C. Ayar[a,b,c], Michelle R. Heusser[c,d], Clara Bourrelly[c,d], and Neeraj J. Gandhi[a,b,c,d,e,1]

Edited by Ranulfo Romo, El Colegio Nacional, Mexico City, Mexico; received March 5, 2023; accepted August 23, 2023

Sensorimotor transformation is the process of first sensing an object in the environment and then producing a movement in response to that stimulus. For visually guided saccades, neurons in the superior colliculus (SC) emit a burst of spikes to register the appearance of stimulus, and many of the same neurons discharge another burst to initiate the eye movement. We investigated whether the neural signatures of sensation and action in SC depend on context. Spiking activity along the dorsoventral axis was recorded with a laminar probe as Rhesus monkeys generated saccades to the same stimulus location in tasks that require either executive control to delay saccade onset until permission is granted or the production of an immediate response to a target whose onset is predictable. Using dimensionality reduction and discriminability methods, we show that the subspaces occupied during the visual and motor epochs were both distinct within each task and differentiable across tasks. Single-unit analyses, in contrast, show that the movement-related activity of SC neurons was not different between tasks. These results demonstrate that statistical features in neural activity of simultaneously recorded ensembles provide more insight than single neurons. They also indicate that cognitive processes associated with task requirements are multiplexed in SC population activity during both sensation and action and that downstream structures could use this activity to extract context. Additionally, the entire manifolds associated with sensory and motor responses, respectively, may be larger than the subspaces explored within a certain set of experiments.

oculomotor | sensorimotor | superior colliculus | dimensionality reduction | saccade

Significance

Sensorimotor transformation is a process humans perform countless times a day, for example, when we look at or reach for objects of interest. Many brain areas register a sensory stimulus and convert the stimulus-related information into an appropriate motor command. Deficits in sensory and/or motor processes are implicated in neurological dysfunctions like attention deficit disorders. We investigated how the context of behavioral tasks impacts patterns of population activity during sensation and action. Dimensionality reduction techniques reveal that context can impact both the sensory- and movement-related transient activity patterns in the population of superior colliculus neurons. This insight is not readily identifiable in single-unit recordings and thus motivates the use of population-level analysis to investigate neural function.

Envision a stopped car in a turn-only lane at an intersection. When the traffic signal turns green, the driver will either make the turn immediately or wait until oncoming traffic and pedestrians in the crosswalk clear. In both cases, the primary sensory input and motor output—traffic light turning green and making the turn, respectively—are categorically identical, but cognition contributes to the overall process. Executive control clearly impacts when the movement is produced, but whether the neural signals underlying sensation and action are also altered remains unclear (1–3). Such conditions can be simulated in the laboratory environment and combined with neurophysiological experiments.

We used the wealth of knowledge in the oculomotor system to study contextual impact on the transient sensory and motor content representations in the superior colliculus (SC) during visually guided saccades. Cognitive context can be manipulated through two behavioral tasks that are akin to the aforementioned scenarios. The visually guided delayed saccade task, which we will refer to as the "delay task," requires executive control to withhold the eye movement until another cue grants permission. This condition prolongs the temporal delay between the sensation and action aspects of the task. The "gap task," in contrast, requires immediate action. It creates a predictable situation in which movement preparation can precede stimulus onset, which can reduce the reaction time (4–6).

Situated at the roof of the brainstem, the SC is a topographically organized, laminar structure that encodes sensory and motor information along its dorsoventral axis (7–10). A population of neurons will emit a burst of spikes when a visual stimulus is presented in their response fields. The initial response is largely exogenously driven, reflecting "sensation" or registration of the stimulus. Just before saccade onset, an ensemble of SC neurons will produce another burst of spikes. This is the "action" command that generates the eye movement. Most neurons that produce a movement-related burst also exhibit a sensory (visual) burst and thus are called visuomotor neurons. The sensory and motor bursts are temporally separated from each other in the delay task but can occur in close temporal proximity and even overlap partially in the gap task (6, 11). Previous neurophysiological studies of SC have mainly used single electrodes. The visual burst produced during the gap task is generally higher than in the delay task, purportedly because the bottom–up visual burst adds to a gradually accumulating, top–down preparatory signal that reflects

Author contributions: E.C.A., M.R.H., and N.J.G. designed research; C.B. performed research; E.C.A. and M.R.H. analyzed data; and E.C.A., M.R.H., and N.J.G. wrote the paper.

Competing interest statement: N.J.G. is on the advisory board for Neuraville, LLC.

This article is a PNAS Direct Submission.

[1]To whom correspondence may be addressed. Email: neg8@pitt.edu.

This article contains supporting information online at https://www.pnas.org/lookup/suppl/doi:10.1073/pnas.2303523120/-/DCSupplemental.

Published September 25, 2023.

the predictability of the target location and onset time (6, 12–15). The motor burst, in contrast, is essentially comparable across tasks, provided that the saccade is directed to a visible target (12, 16, 17) We confirmed that single units we recorded via laminar multicontact electrodes followed these established firing rate characteristics.

Importantly, we aimed to determine whether a targeted population-level examination, which takes into account the covariability of spiking patterns across simultaneously recorded SC neurons, can tease apart across-task differences better than traditional analysis that averages the firing rates across individual neurons. Similar techniques have been successfully implemented in the analysis of cortical activity (18–21), which provided us a secondary rationale for studying the SC, an area with much less heterogeneity in firing rate patterns across neurons (10). Thus, despite the apparent homogeneity across neurons in any given recorded SC population, can more be gained by studying the correlated activity patterns across neurons rather than averaging the firing rates of single neurons? To answer this question, we applied machine learning–inspired dimensionality reduction techniques to identify the latent factors and subspaces spanned by the visual and motor responses of neural populations in both tasks. Our goal was to determine whether the population-level representation of sensory and motor responses in SC is task dependent, in contrast to single-unit firing patterns which are unable to distinguish task context during the motor response. Discriminant analyses were used to determine the separability of the response distributions across epochs (content) and tasks (context). The findings verified that the visual responses were separable from motor responses in the delay task (22), and a similar result was observed for the gap task. We also found across-task separability in both visual and movement responses, the latter of which was not expected based on single-unit analyses. We interpret the findings to indicate that cognitive context can impact both exogenous and endogenous components of the sensory response as well as the transient features of the motor burst and that sophisticated statistical methods applied to simultaneously recorded neural activities are more effective at revealing the distinction.

Results

We set out to characterize features of population activity in the SC in two commonly used behavioral tasks (Fig. 1*A*) to better understand contextual effects on neural signatures of sensation and action (content). In each session, we used a laminar probe to record spiking activity simultaneously from a small ensemble of neurons along the dorsoventral axis of SC while the animal produced saccades to a target presented at either the preferred location associated with the track or the diametrically opposite position, although all analyses were limited to the former subset. In each task, both sensory (visual) and motor bursts are evident in the activities of same SC neurons as the animal perceives and subsequently makes a saccade toward the optimal response field. The structure of the delay task imposes a clear temporal separation between the two epochs while the gap task creates a situation in which the two bursts can overlap or even merge into one (Fig. 1*B*). The sensory response was strongest in the superficial layers and decreased gradually for deeper layers (10, 22, 23). The motor burst was maximal in the intermediate layers and decreased gradually in neurons both above and below. These systematic patterns reveal the homogenous feature of SC neurons relative to the cortex. Fig. 1 *C* and *D* compares each neuron's visual and motor responses between the two tasks. The visual response was measured 160 ms (delay task) or 140 ms (gap task) after target onset, which closely aligned with the peak of the transient response. The motor response was sampled at saccade onset, which was generally synchronous with the peak of the movement-related burst. The insets show for each task the temporal discharge profiles averaged across all neurons in the two epochs. In agreement with previous studies, the visual responses were statistically significantly different across tasks (paired t test, $P < 0.001$) while the motor bursts were not (paired t test, $P = 0.87$). Additionally, movement features, namely peak velocity and saccade amplitude, were also not statistically different between the two tasks (*SI Appendix*, Fig. S1).

This experimental configuration creates conditions for direct assessments of single neuron and population-level analyses for both content and context. Both sets of analyses should differentiate sensory from motor responses within a task, given the systematic organization of these features across neurons at different depths. Population-level analysis should also confirm that the visual response is different across the two tasks, given the individual neuron effect shown in Fig. 1*C*. The key test then is whether population activity differentially encodes the motor burst in the two conditions, given that both the firing rates across individual neurons and the accompanying movement features are mean-matched (Fig. 1*D* and *SI Appendix*, Fig. S1).

Dimensionality reduction techniques effectively change the coordinate system of the observed data. We used it to represent spike trains or spike density waveforms recorded simultaneously from n neurons as n latent (unobservable) time-varying factors for each trial. Each latent factor is a weighted linear combination of the individual neurons' activities, where the weights maximize the variance across neurons. Every neuron has a constant weight contribution to each factor. The weight can change across factors, but it is constant for all time points and trials for any given factor (*Materials and Methods*). The factors are generally ordered according to the amount of variance they capture. Typically, additional analysis is focused on the $m < n$ latent factors that account for a large portion of the variance. We specifically used Gaussian Process Factor Analysis (GPFA) for dimensionality reduction because it smooths the time-varying latent factors to yield less noisy and better visualizable waveforms (24). Fig. 2*A* plots the time courses of the top three, trial-averaged latent factors for each task. For our SC data, the first latent factor qualitatively resembles the firing rate profile because the bursts account for the large variance (the polarity of the signal is not crucial because weights can be positive or negative). The second factor, in contrast, features opposite deflections in the visual and motor epochs, although this is more appreciable when the two periods are separated in time as in the delay task. The third and higher dimension factors show minimal or negligible modulation. For each session, the absolute projection weights of each neuron were gathered for each factor and all neurons were sorted by their projection weight magnitudes (Fig. 2*B*). For all factors and sessions, we found that many neurons contributed to the variance, indicating that any resulting separation in activity was not dominated by a small number of individual neurons but rather due to the combined activity of a neural population.

The top 4 latent factors accounted for at least 95% of the variance across neurons in the firing rate profiles for 18 out of 20 datasets (25). Unless noted otherwise, we chose to analyze only the top 3 latent dimensions because the third and higher dimensions do not show much modulation during either epoch. This low dimensionality also facilitates inspection and comparison of the factors across different conditions in a three-dimensional state space. For instance, imagine the three factors in Fig. 2*A* plotted in state-space form. It would effectively be a trajectory that evolves

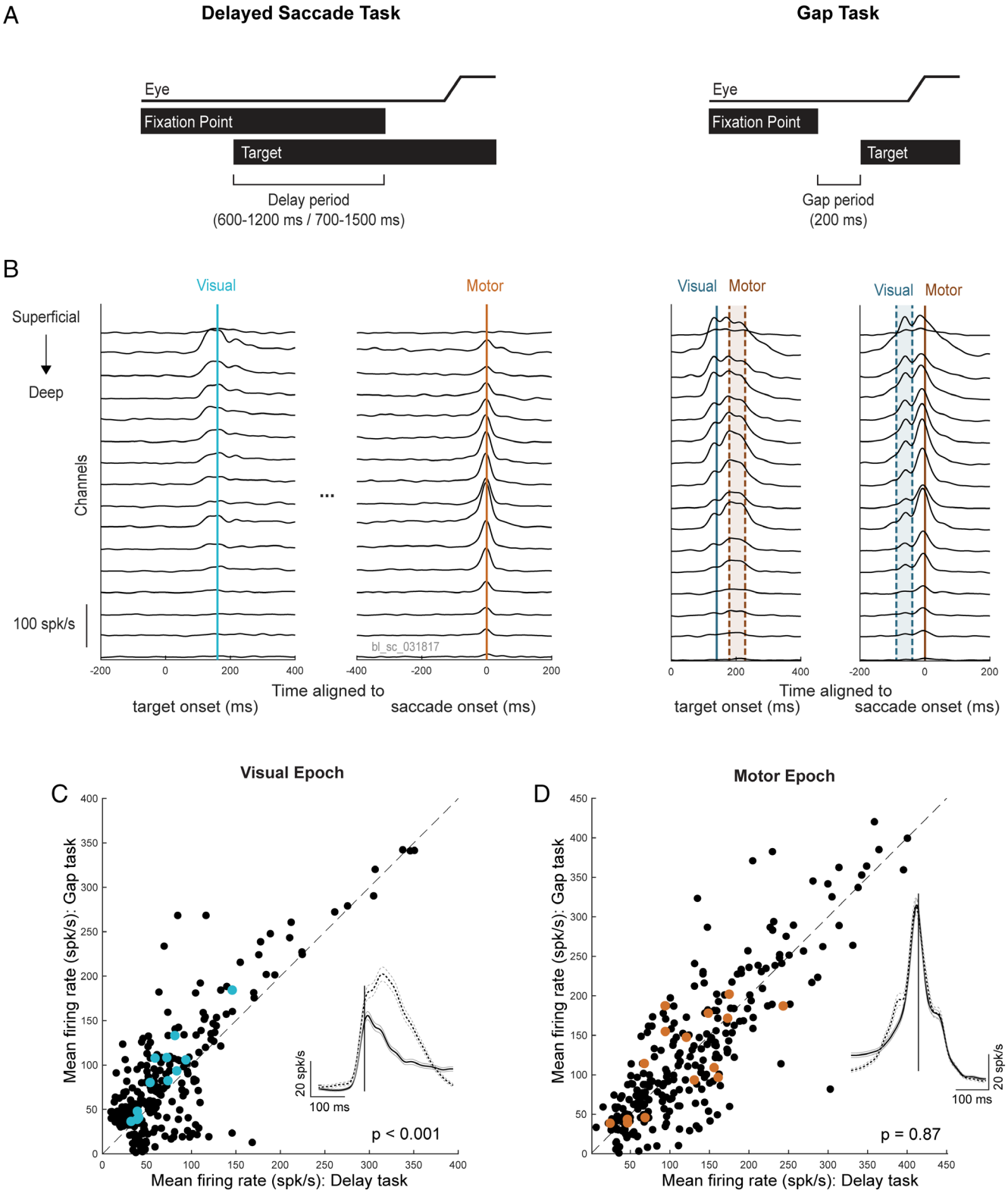

Fig. 1. Overview of tasks and corresponding neural firing rate properties. (*A*) Temporal representations of the delay (*Left*) and gap (*Right*) tasks. Each has identical key events (fixation on a central point, subsequent target appearance, and instructed saccade), but they progress with different timelines. (*B*) Multiunit activity averaged across trials for each recorded channel of one example session arranged from superficial to deep along the dorsoventral axis of the SC. The activity on each channel is aligned to target onset (*Left* panel of each task) and saccade onset (*Right* panel of each task). The traces are shifted vertically to reflect the recording channel. Activity around the peak of the visual and motor bursts are indicated by blue and brown vertical lines, respectively. For the gap task, the shaded rectangle in each panel corresponds to ±1 SD around the mean saccade onset time (*Left*) or visual burst time (*Right*). (*C* and *D*). A comparison of single neuron firing rates across all recorded populations at the time of the solid vertical lines in the visual (*C*) and motor (*D*) epochs between the delay (*x* axis) and gap (*y* axis) tasks. Only neurons reaching a threshold of 30 spikes per second in at least one of the two epochs are shown and included in statistical analyses. Across all neurons, single-unit firing rates differ between tasks during the visual epoch but not the motor epoch (paired *t* test). Firing rates of the example population in (*B*) are highlighted as colored points. *Insets*: Firing rate profiles in the visual (*C*) and motor (*D*) epochs averaged across all trials of the delay (solid lines) and gap (dashed lines) tasks and averaged across all included neurons. Vertical lines indicate 140 ms after target onset (*C*) and saccade onset (*D*), the time point used for further analyses.

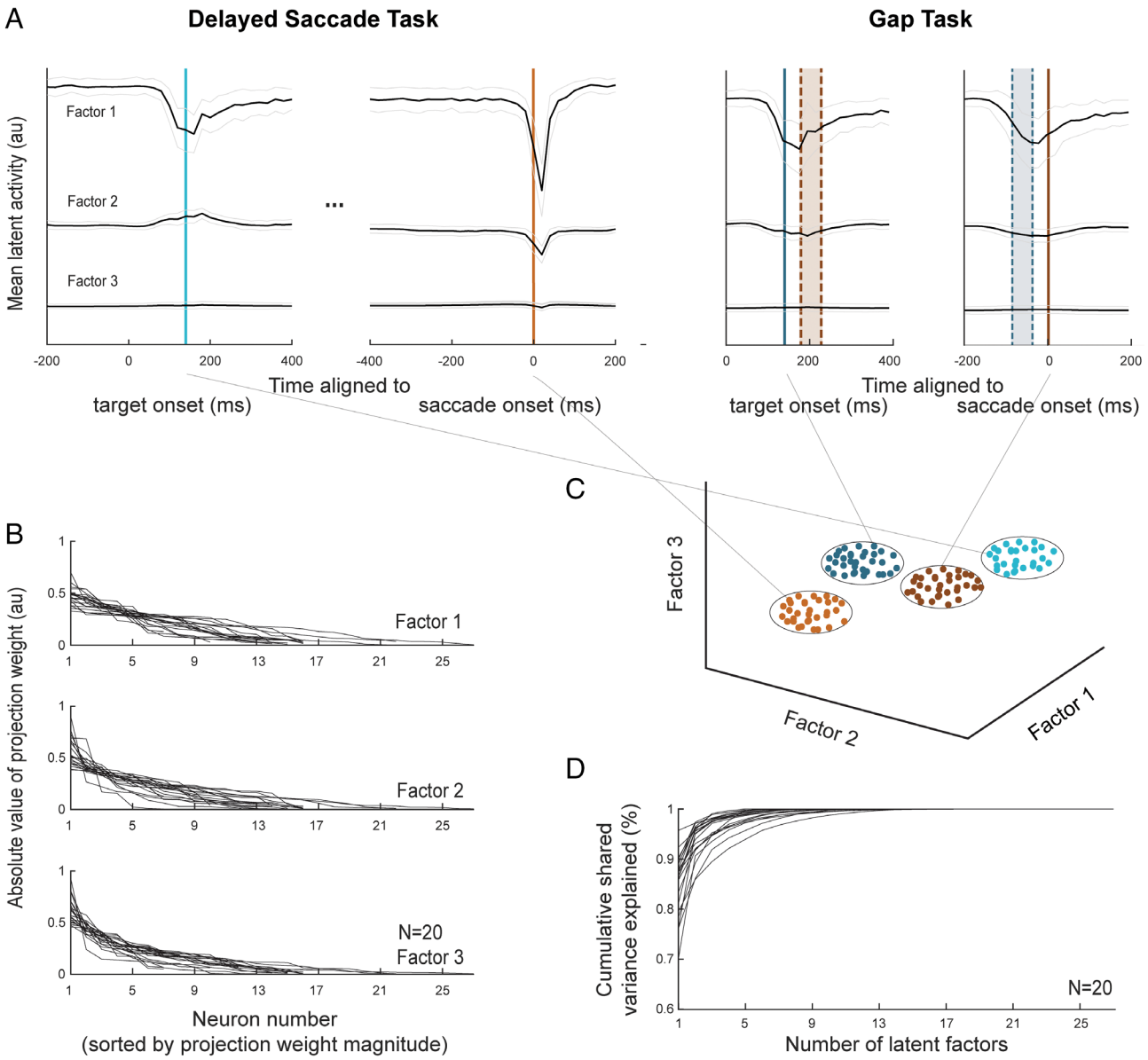

Fig. 2. Overview of dimensionality reduction to view population activity in a state-space framework. (*A*) Magnitude of trial-averaged latent activity (black trace) ±1 SD (gray traces) across time for each of the first three factors, separated by arbitrary vertical offset, retained after performing GPFA on spike-sorted population activity. We used the same conventions and example session here as described in Fig. 1*B*. Activity around the peak of the visual and motor bursts are indicated by blue and brown vertical lines, respectively. For the gap task, the shaded rectangle in each panel corresponds to ±1 SD around the mean saccade onset time (*Left*) or visual burst time (*Right*). (*B*) Projection weight of all neurons into each latent factor sorted from the neuron with the largest projection weight to that with the smallest for each session. Each session contributes one trace to each factor (N = 20). Most sessions have many neurons contributing to each latent factor; therefore, the three-dimensional latent values produce a true population-level framework rather than one dominated by a select few neurons. (*C*) Hypothetical subspaces formed by activity during the visual (blue) and motor (brown) time stamps of the delay task (lighter colors) and gap task (darker colors). Envision creating for each trial a three-dimensional trace that produces a spatial trajectory of the top three latent factors. Now extract for each trial the three-dimensional points that correspond to the times marked by the solid vertical lines (visual and motor epochs in both delay and gap tasks) in *A*. The ellipses reflect one potential distribution of subspaces where each dot corresponds to a given trial. It is a hypothetical distribution, not intended to reflect the traces in *A*. Other possibilities include nearly identical or partially overlapping subspaces (not shown). (*D*) Cumulative amount of shared variability across neurons explained by lower-dimensional models compared to the full-dimensional model (full dimensionality is equivalent to the number of neurons in the population). Each session is again represented by a single trace. A high amount of covariability in neural activity patterns can be explained by only a few factors for the majority of sessions.

with time. We could then determine whether the "subspaces" occupied during the visual and motor time stamps (solid vertical lines) for both delay and gap tasks overlap completely, partially, or not at all. Fig. 2*C* illustrates a hypothetical case in which all four subspaces are distinct. We implemented a two-class linear classifier to quantify the separability between each pair of neural subspaces. We specifically tested the separability of activity 1) across epochs within each task (i.e., visual vs. motor activity; content), 2) across tasks within each epoch (i.e., delay vs. gap activity; context), 3) across epochs when both tasks are combined (content), and 4) across tasks when both epochs combined (context).

Within-Task, Across-Epoch Analysis. Determining whether patterns are distinct across epochs for each task may give intuition as to whether there are unique neural signatures during the sensation and action periods of sensorimotor transformation. We used linear discriminant analysis (LDA), which produces a plane that maximizes the separability of the two subspaces considered for each analysis (*Materials and Methods*). For our first analysis,

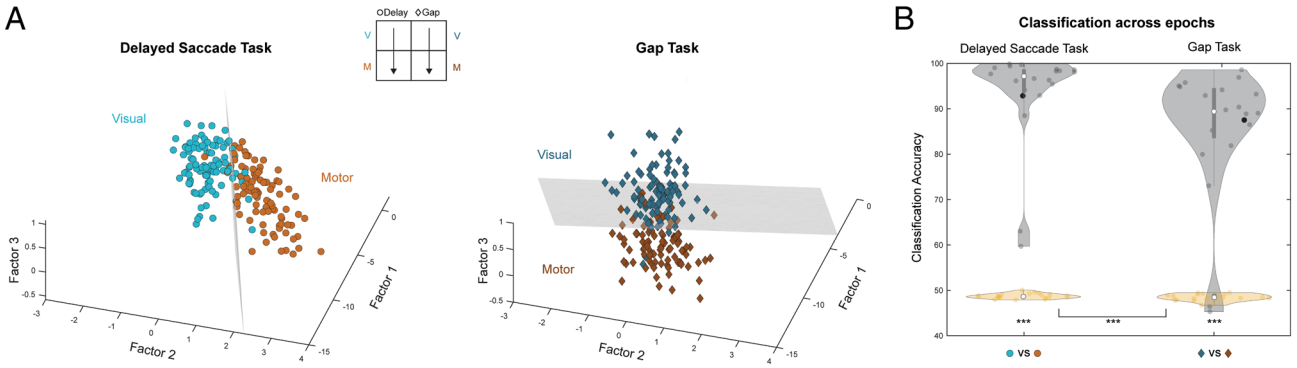

Fig. 3. Separability of visual and motor subspaces within a task condition. (*A*) Clusters or subspaces of latent activity in the three-dimensional state space for an example session taken from the visual (light/dark blue) and motor (light/dark brown) epochs as defined in Fig. 1*B*. Each point represents the latent activity in a 20-ms window taken from an individual trial of the delay task (*Left*) or gap task (*Right*). The plane of maximum separability between the two clusters found through a LDA model is denoted by a gray rectangle. The separability between the visual and motor subspaces was determined independently for each task. (*B*) Violin plot of classification accuracy between the visual and motor epochs for the delay (*Left*) and gap (*Right*) tasks for all 20 sessions. Individual sessions are represented by gray points, with the example session indicated by a black point. A traditional box and whiskers plot is overlayed on the vertical meridian. The beige violin plot and associated points indicate classification accuracy of each session after shuffling the epochs. Significance is reported both within and across distributions (one-tailed Wilcoxon signed rank test against the median of the chance level distribution and two-tailed paired Wilcoxon signed rank test, respectively). Accuracy in distinguishing visual from motor latent activity is significantly above the median of the chance level distribution for both tasks ($P < 0.001$).

we used "visual" and "motor" categories to classify the data. As expected from previous work (22), the visual subspace is separable from the motor subspace for the delay task (light blue and light brown circles, respectively, in Fig. 3 *A*, *Left*). We report here that the visual and motor subspaces are also distinct in the gap task (dark blue and dark brown diamonds, respectively, in Fig. 3 *A*, *Right*). This separability likely reflects the varying contributions of each neuron during each epoch, as some SC neurons have larger visual bursts than motor bursts (and vice versa). Overall, regardless of the presence (or lack thereof) of an imposed delay, this session's population activity patterns are distinct between the sensory and motor epochs.

The LDA classifier performed significantly above chance level across all sessions (one-tailed Wilcoxon signed-rank test, $P < 0.001$), with a mean (±1 SD) classification accuracies of 93.2% (±2.19%) for the delay task and 85.3% (±2.87%) for the gap task (Fig. 3*B*). The classifier was significantly more accurate in distinguishing between sensory- and motor-related activity within the delay task than within the gap task (paired Wilcoxon signed-rank test, $P < 0.001$). These results suggest that the between-epoch subspaces representing content are more separable within the delay task, likely due to the imposed delay period that clearly separates the visual and motor epochs. Overall, the separability of visual and motor patterns within a specific behavioral context is characteristic of a unique neural population activity pattern during the respective epochs. As a note, when classifying across epochs, retaining more latent factors does not qualitatively affect subspace separability; rather, the classification accuracies plateau (*SI Appendix*, Fig. S2*A*).

We also performed factor analysis (FA) using varying Gaussian smoothing kernels (width = 1, 6, and 10 ms) to ensure that the inherent temporal smoothing component of GPFA did not artificially constrain the separability between visual and motor activity in the gap task when the activity patterns may diverge at a short temporal scale. When running FA with a small smoothing kernel (1 ms) before performing LDA, the classifier still performs significantly above chance level (*SI Appendix*, Fig. S3*A*). With smoothing kernels of 6 ms and 10 ms, the results are even more similar to those of GPFA (*SI Appendix*, Fig. S3 *B* and *C*). This control analysis indicates that our results do not hinge on the exact decoding algorithm and parameters used.

Within-Epoch, Across-Task Analysis. The analysis was then extended to compare patterns of activity between the two tasks for the same epoch. We specifically evaluated whether neural signals underlying sensation and action are represented in a different manner depending on the context or trial type. In Fig. 4*A*, one can see that for the same example session as in Fig. 3, there is indeed a separation during the visual epoch between the patterns exhibited by this neural population in the gap and delay tasks (blue circles and diamonds, respectively). A similar effect was also found for the motor epoch (brown circles and diamonds). Again, employing a two-class linear discriminant classifier (with "delay" and "gap" categories) to quantify the subspace separability for all sessions, we found the classification accuracy to be significantly above chance level during both epochs (one-tailed Wilcoxon signed-rank test, $P < 0.001$). The across-session mean (±SD) classification accuracies were 77.9% (±3.82%) for the visual epoch and 80.8% (±3.36%) for the motor epoch (Fig. 4*B*). There was no significant difference in the between-task separability of visual-related or motor-related activity (paired Wilcoxon signed-rank test, $P = 0.24$). The presence of two distinct subspaces across tasks suggests that the way in which content-related signals are processed in the SC is unique to the cognitive demands of a given task. Retaining more than three latent factors did improve gradually the observed separability between subspaces (*SI Appendix*, Fig. S2*B*) but did not qualitatively change the result, and results were robust to the use of a different dimensionality reduction algorithm altogether (*SI Appendix*, Fig. S3 *D–F*). Separating the neurons recorded in each session into subpopulations according to depth in the SC does not qualitatively change these results either; whether the subpopulations are taken from sequential channels or from the most superficial and deepest channels, classification accuracy remains above chance level in all cases (*SI Appendix*, Fig. S4).

Combined Across-Task and Across-Epoch Analyses. We then applied LDA to determine whether all visual activity is distinct from all motor activity regardless of the task condition. In other words, do the visual patterns from both tasks reside in a larger, encompassing space that is separable from the space in which their motor patterns reside in a low-dimensional state space. In Fig. 2*C*, one can visualize this as drawing a larger ellipse around the two blue ellipses (representing visual activity) and determining

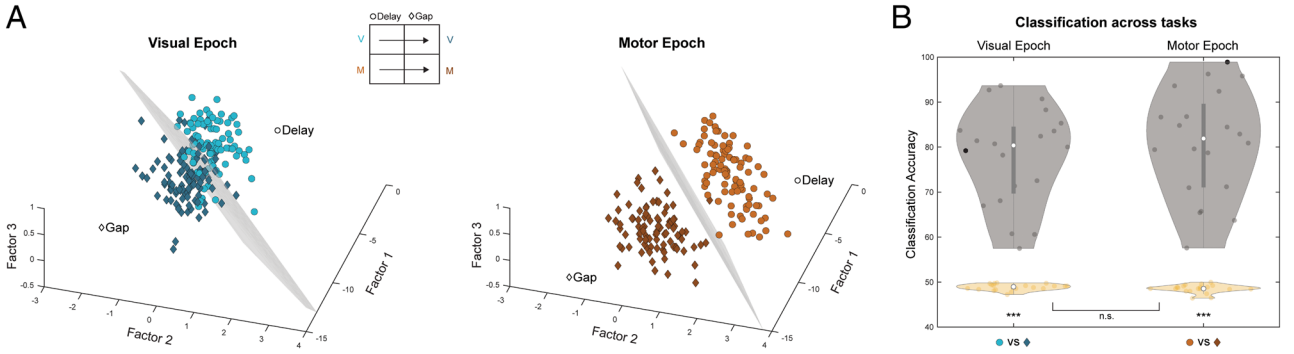

Fig. 4. Separability of task-specific representations within an epoch. (*A*) Same conventions as in Fig. 3*A* but with planes of maximum separability computed between activity from delay (circles) and gap (diamonds) trials for the visual (*Left*) and motor (*Right*) epochs. (*B*) Same as in Fig. 3*B* but for accuracy in classifying task condition during the visual (*Left*) and motor (*Right*) epochs. Accuracy in distinguishing activity from the delay task from that during the gap task is significantly above the median of the chance level distribution for both epochs ($P < 0.001$).

whether this larger ellipse is distinct from a larger ellipse drawn around the two brown ellipses. Fig. 5*A* shows for the same example session the two-dimensional plane that best separates all visual activity from all motor activity. Across all sessions, there are distinct patterns of activity between the visual and motor epochs with a mean classification accuracy of 87.5% (±1.98%), which is significantly above chance level (one-tailed Wilcoxon signed-rank test, $P < 0.001$) (Fig. 5*C*). We also found that a single plane can

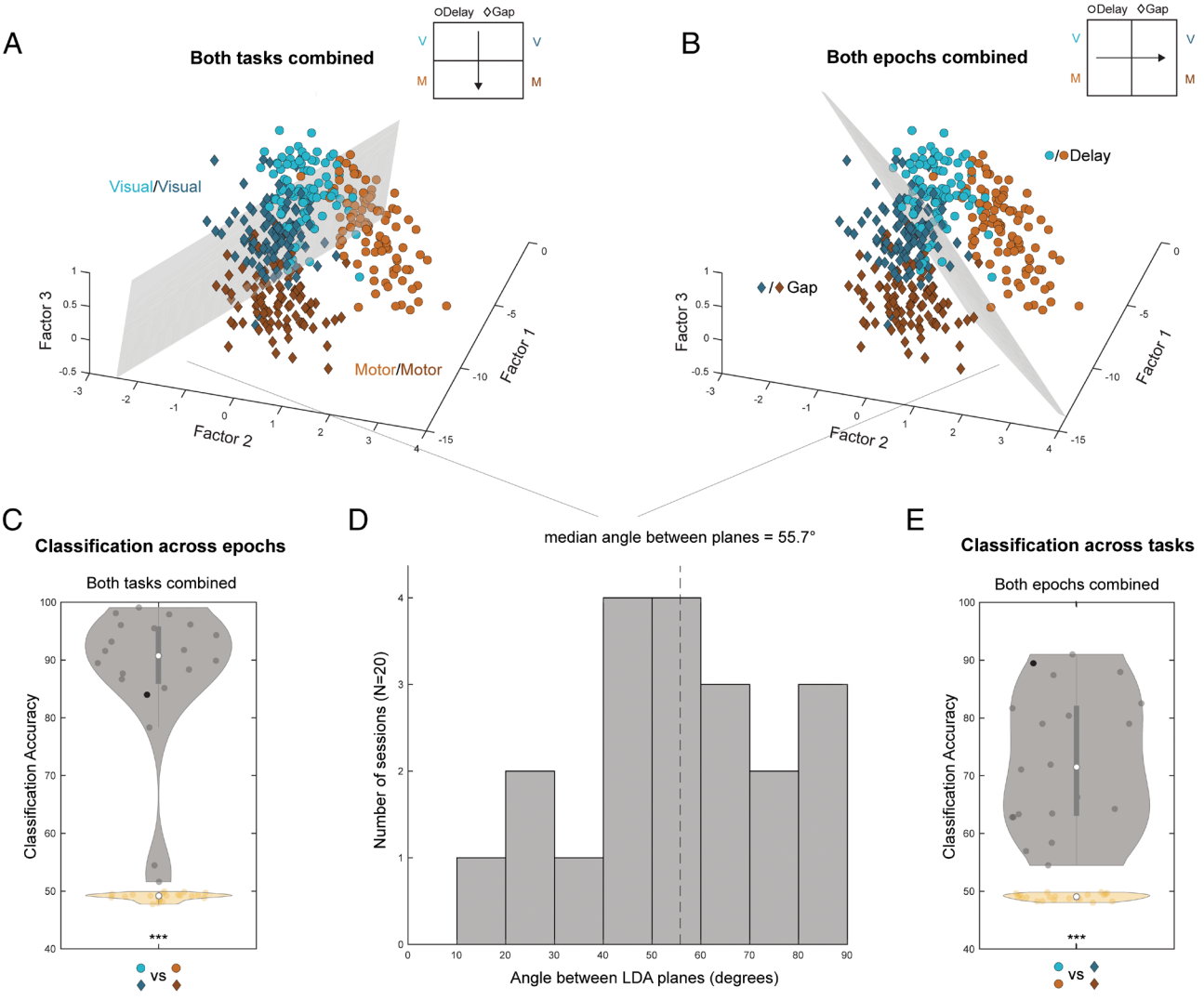

Fig. 5. Combined separability of subspaces across epochs or tasks. (*A* and *B*) Same as in Fig. 3*A* but for (*A*) the separability of activity between the visual (blue) and motor (brown) epochs when activity is pooled across both tasks or (*B*) the separability of activity between delay (circles) and gap (diamonds) tasks when activity is pooled across both epochs. (*C*) Same as in Fig. 3*B* but for accuracy in classifying visual and motor activity when both tasks are combined. The beige violin plot and associated points indicate classification accuracy of each session after shuffling the epochs. In both cases, the separability is significantly above the median of the shuffled distribution ($P < 0.001$). (*D*) Histogram across sessions of the angle between two planes that maximally separate the content (e.g., gray plane in *A*) and context (e.g., gray plane in *B*) subspaces. (*E*) Accuracy of classifying task condition when both epochs are combined, following the format of panel *C*.

considerably divide delay and gap task activity regardless of the epoch from which the activity came (Fig. 5*B*). This classifier also performed significantly above chance level across sessions (one-tailed Wilcoxon signed-rank test, $P < 0.001$), with a mean accuracy of 72.7% (±2.85%) (Fig. 5*E*).

In order to determine whether SC populations encode content (visual vs. motor) and context (delay vs. gap) independently, we computed for each population the angle between the two vectors normal to each LDA plane. Fig. 5*D* shows the distribution of these angles across all sessions. The median angle between decoding axes was 55.7°, indicating a distinct but not orthogonal representation of content and context in these SC populations. Similar values were found using FA with kernel widths of 1 ms, 52.9°; 6 ms, 63.0°; and 10 ms, 62.7°.

Single-Unit vs. Population-Level Frameworks. Next, we evaluated whether there was any correlation between classification accuracies found with the machine learning approach and statistical significance obtained by comparing the peak firing rates. Consider the example session shown in Fig. 1*B*. When pooling the firing rates of all recorded neurons on this session, the activity was differentiable between tasks during the visual epoch but not the motor epoch (colored dots in Fig. 1 *C* and *D*). If the GPFA plus LDA approach were redundant (i.e., depending solely on firing rate differences), the classification accuracy for this session would be high during the visual epoch but not the motor epoch. On the contrary, this session exhibited moderate subspace separability during the visual epoch (79.2%) but had the highest subspace separability during the motor epoch out of all included sessions (98.9%). Comparing the significance levels of across-task firing rates differences on individual sessions with their respective subspace classification accuracies (*SI Appendix*, Fig. S5 *A–C*), we found a moderate correlation during the motor epoch (Pearson correlation, R = −0.54; *t* test, $P = 0.01$) but not in the visual epoch (R = −0.08; *t* test, $P = 0.74$). Subspace classification accuracy persisted but without a correlation even earlier in the visual burst, when firing rates in the two tasks were mean-matched (R = −0.11; *t* test, $P = 0.65$).

Correlations in activity of simultaneously recorded neurons can also be informative of information relevant to a task (26–28). We also correlated the subspace classificaiton accuracies with statistical significance levels of across-task covariability among neurons on individual sessions (*SI Appendix*, Fig. S5 *D–F*). We found moderate but not significant correlations during the motor epoch (Pearson correlation, R = −0.26; *t* test, $P = 0.28$), visual epoch (R = 0.04; *t* test, $P = 0.87$), and when the visual response was matched (R = −0.23; *t* test, $P = 0.32$). Thus, there is not a strict correlation between classification accuracy and the statistical significance value based on the distribution of individual sessions. This is because the dimensionality reduction exploits various features—firing rate and variance being just two of them—to determine the weights and the latent factors.

Nogueira et al. (29) showed that the changes in population activity across tasks (population signal, PS) and the inverse covariability along the PS axis (projected precision, PP) are more informative about information encoding and behavior than modulation in global activity (GA) and mean pairwise correlation (MPC). We therefore repeated their conditioned bootstrapping approach to further explore which of these four statistical features contribute to the observed distinguishable patterns of activity across tasks (*Materials and Methods* and *SI Appendix*, Fig. S6). When comparing across the delay and gap tasks during the visual epoch (Fig. 6*A*), the percentage improvement in decoding performance (DP% change) was 2.57% (±0.65%) conditioned on MPC, 2.49% (±0.64%) on GA, 4.82% (±1.68%) on PS, and 5.13% (±1.09%) on PP. The results are similar when comparing across tasks during the motor epoch (Fig. 6*B*): 2.28% (±0.96%) on MPC, 2.30% (±0.88%) on GA, 5.04% (±1.62%) on PS, and 4.80% (±1.44%) on PP. We found the DP% changes to be significantly above 0 in each condition for all statistical features (one-tailed Wilcoxon signed-rank test, $P < 0.01$), suggesting that all features contribute to the separation of patterns of activity. Similar to Nogueira's findings, PS and PP have significantly different distributions than MPC and GA (Wilcoxon signed-rank test, $P < 0.01$). Thus, these statistical features each play a potential role in the high classification of context we observed during the visual and motor epochs, although PS and PP have a larger contribution.

Finally, we followed the procedure of Leavitt et al. (30) and performed our classification analysis after excluding untuned neurons (*Materials and Methods*). The use of "untuned" is not to be confused with the more standard tuning definition referring to whether the neuron is tuned for a spatial region of visual space or a span of saccade vectors. Here, this term indicates that the distribution of peak activity in a given epoch (content) is statistically similar for both tasks (context). An average of 2.5 neurons per

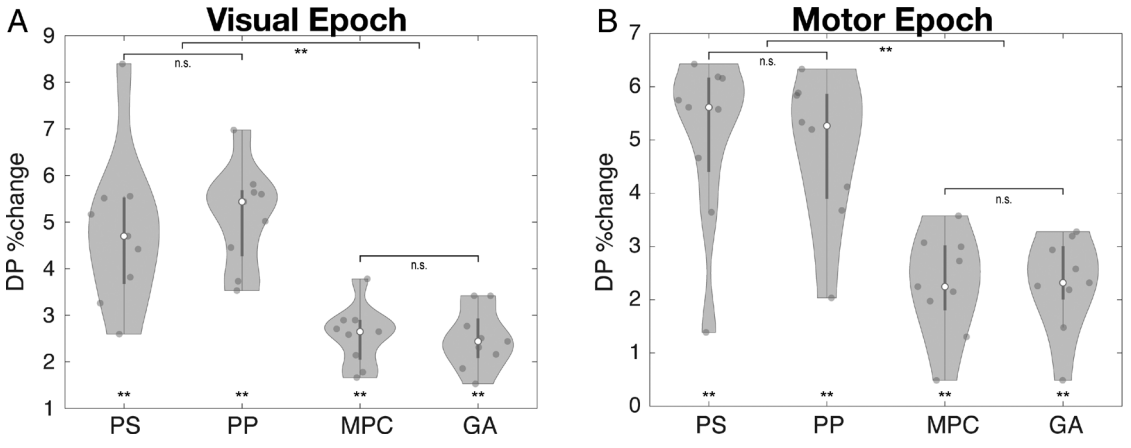

Fig. 6. Separability of patterns of neural activity during sensation and action mostly depends on statistical features PS and PP. For the visual (*A*) and movement (*B*) epochs, we computed the decoding performance change (DP% change) when conditioning on either PS, PP, MPC, or GA. Significance is reported both within and across distributions (one-tailed Wilcoxon signed rank test against 0 and two-tailed paired Wilcoxon signed rank test, respectively). In both epochs, the DP% change is significantly above the 0 ($P < 0.01$) for all statistical features.

dataset were considered untuned, and the range was 0 to 7 neurons across datasets. We did not find any significant difference in the decoding performance (*SI Appendix*, Fig. S7) during either epoch after excluding untuned neurons from the population. Thus, untuned neurons do not have significant contribution to the observed separation of patterns of population activity.

Discussion

The SC is a central hub in the neuraxis that transforms sensation into action while also incorporating cognition (8, 9, 31–33). The general chronological order is that stimulus presentation induces a transient, exogenous burst of activity in SC neurons. Endogenous processes then contribute to SC activity, usually in the form of low-frequency modulation. This modulation has been linked to various cognitive features, as dictated by the experimental paradigm (34). Some examples include spatial attention (35), motor preparation (36, 37), antisaccade generation (38), decision-making (39, 40), visual search (41, 42), reward processing (43), and remapping (44, 45). The culmination of the contextual processing leads to another burst of activity that produces a movement. Crucially, there is little consideration of context-dependent processing on the initial sensory response and even less on the final motor burst. Moreover, most studies have analyzed firing rates of individual SC neurons and then pooled the results by averaging the measures across neurons. The ability to record activity from many neurons simultaneously permits a higher-order, dynamical systems analysis that examines covariability across neurons (24). Such efforts have yielded deeper insights into neural systems, although this technique has scarcely been applied to brain structures involved in producing visually guided eye movements; see refs. 22, 25, and 46 for notable exceptions.

We therefore explored how neural populations in the SC encode two different forms of information—content (sensation and action) and context (two comparable behavioral tasks). We designed an experiment in which one content signal is different and the other similar across the two contexts when analyzed through the lens of average firing rates of individual neurons. We expected that processing the "different" content signals through machine learning algorithms would return high classification accuracy; this was effectively our internal control. The key question was what do we get when we process the "similar" content signals through the same algorithms? Our "sensory" content signal was the across-trial average activity measured 140 ms after target onset (solid, vertical blue lines in Fig. 1*B*); this corresponds closely with the time of peak visual response. Our motor content signal was the activity at saccade onset (solid, vertical brown lines in Fig. 1*B*), which also aligned roughly with the peak of the motor burst. Next, we had to decide which content signal should be similar and which one different. We initially considered matching the sensory burst. This is easily achieved by randomizing the visually guided delayed saccade task with, for example, a memory-guided task, as both follow a similar time course. We also contemplated using the step task. In such cases, however, the animal would not know the context at the time the visual stimulus was presented. That would be a flaw in the design because the contextual information must have the opportunity to influence both content signals. Thus, we concluded that the correct choice was to match the motor burst and allow the sensory burst to be different across two tasks. This led us to contrast the gap task against the visually guided delayed saccade task. Indeed, the peak firing rate grouped across neurons was different during the visual burst (Fig. 1*C*) but similar for the motor burst (Fig. 1*D*) between the two tasks. With these data in hand, we found the opportunity to test what additional insights are gained with analyses of neural activity measured simultaneously across an ensemble of neurons.

First, we compared the population activity patterns during the periods of sensation and action and observed content-specific encoding in both the delay and gap tasks. The result (Fig. 3) matches closely with our intuition based on the known properties of SC neurons. Although we recorded primarily visuomotor neurons (i.e., those exhibiting both a transient visual and motor burst), the relative firing rate of each individual neuron during each epoch is imbalanced. Along the dorsoventral axis of the SC, neurons located more superficially respond more strongly to the appearance of a visual stimulus, while deeper neurons fire more strongly for the generation of a saccade (10, 47, 48). Since subspaces are formed by a weighted linear combination of activity across all recorded neurons, it logically follows that the population-level representations are distinct across epochs. This result is consistent with the notion that the trajectory formed by the neural population traverses through different regions of the state space as the trial transitions through stages of sensation, cognition, and action (18, 25, 46, 49) and is confined to lower-dimensional "manifolds" (50). The present study therefore builds another case for the importance of characterizing neural activity through a measure that accounts for the relationship between neurons rather than by averaging the signal across all neurons, as is the standard in single-unit studies.

We then quantified the content subspaces formed by population activity during the delay and gap tasks. During both the sensory period (equivalently, around the peak time of transient visual-related activity) and the motor period (around saccade onset), the subspace formed by the population activity pattern diverged across the two tasks, consistent with a context-specific representation (Fig. 4). For the visual epoch, this is likely due to the interaction or addition of bottom–up visual transient with movement preparation-related activity that begins accumulating in the gap period, particularly when target locations and onset times are largely predictable (6, 12, 15, 36, 51), which is the case in our experiments. This accumulating activity can even be observed in early visual areas (52), which arguably serves to induce a different state in the sensorimotor circuitry by the time of target presentation and impacts the subsequent visual response in the gap task. For matched behavioral metrics and identical stimulus conditions, the saccade-related motor burst of SC neurons is thought to be task invariant as long as the target remains illuminated (12, 17), although target modality and features are known to also modulate the burst (53–55). Thus, we were surprised by the separation of motor subspaces across the two tasks for the identical target (Fig. 4). We were concerned that temporal smoothing component of GPFA, which prevents large and fast deviations of the neural trajectory, may have compromised occupancy of the actual motor subspace in the gap task because of the temporal proximity of the visual and motor bursts, but we observed comparable results when repeating the analysis with FA, which allows user-defined smoothing of the spike train (*SI Appendix*, Fig. S3). We found that various higher-order, statistical features associated with pairwise covariability of simultaneously recorded neurons contributed to the separation of motor subspaces across tasks (Fig. 6), even though differences are not apparent when firing rate is averaged across all neurons (Fig. 1*D*). Future research should zoom out on a window of time during these bursts and compute values such as signal and noise correlations (29, 30, 56–58) to further explore possible contributions to these observed population-level differences.

For our experimental design, we took considerable inspiration from a study by Churchland et al. in which population activity

patterns during reach preparation were found to be largely conserved across tasks with similar external events but that varied in both temporal and cognitive context (59). Here, we do not report the temporal evolution of neural patterns during the period between sensation and action but rather during the sensation and action periods themselves. Extrapolating our finding that the neural representations in the SC underlying sensation and action were not invariant to context, it would follow that activity patterns in the SC during the sensorimotor transformation process are also distinct across tasks. Additional studies that examine conversion of sensory into motor signals across multiple contexts are needed for oculomotor areas. It would also be valuable to investigate context and content processing across multiple target locations and while incorporating local field potentials (60). We may find that more latent factors may be needed to identify the separable features of context during sensation and action.

Since we found both content- (sensation and action) and context- (two behavioral tasks) related population activity in the SC, we lastly asked whether these two dimensions of information are encoded not only simultaneously but also independently. We found that within the scope of our study, these elements are not fully dissociable, as the planes that divide content 1 (visual burst) from content 2 (motor burst) and context 1 (delay task) from context 2 (gap task) are not orthogonal (Fig. 5*D*). On the other hand, the planes are not parallel, which means that oculomotor areas to and from which the SC relays its signals might still decode task context somewhat separately from sensory and motor signals. In other words, knowing which task is being performed is not necessary for interpretation of epoch (i.e., deciphering whether the SC is signaling for target appearance or initiating a saccade command). Conversely, SC activity carries information about task context regardless of epoch. This dissociation of signals is analogous to a mechanism proposed by Kaufman et al. in which orthogonal encoding of preparatory and motor signals in the dorsal premotor cortex prevents premature arm movement initiation (19). Hence, we believe that the application of dynamical systems approach is a valid and fruitful framework for future research into the representation of sensation and action in the oculomotor system across the multitude of possible behavioral contexts.

Materials and Methods

All procedures were approved by the Institutional Animal Care and Use Committee at the University of Pittsburgh and followed the guidelines of the Public Health Service Policy on Humane Care and Use of Laboratory Animals. Data were collected from two adult male Rhesus monkeys (*Macaca mulatta*, identified as BL and SU) who were trained to perform oculomotor tasks using operant conditioning and surgically prepared under aseptic conditions for neurophysiological recordings from the SC. The recording chamber was tilted 40° posterior with respect to vertical to allow microelectrode penetrations orthogonal to the SC surface. A subset of the data used in this manuscript is an analysis of data reported previously, and additional methodological details can be found there (10).

Experimental Design. Stimulus display and acquisition of behavioral data were controlled by a central, customized program written in LabView architecture (61). Eye position was measured using a camera-based pupil tracker (EyeLink 1000, SR Research, Ltd.) sampled at 1 kHz. Each animal was trained to perform two oculomotor tasks. Every trial was initiated by the presentation of a fixation point at the center of the screen, and the animal was required to direct its line of sight on this stimulus. In the delay task (Fig. 1 *A*, *Left*), a single target was presented at an eccentric location while the monkey continued to fixate the central stimulus. The fixation point was extinguished after a delay period (randomized between 600 and 1,200 ms for monkey BL and 700 to 1,500 ms for monkey SU), permitting the animal to bring its visual axis within two degrees of the target. In the gap task (Fig. 1 *A*, *Right*), the fixation point was first turned off, and a constant 200 ms gap in time lapsed before a single target was presented on the screen. The animal could not break fixation during the gap period but could make the saccade immediately after target onset. In both tasks, the animal received a liquid reward for maintaining fixation within a 2 to 3° window around the final target location for at least 250 ms. For each session, the peripheral target was presented at either the location deemed to be optimal across the neurons on a given track or the diametrically opposite position. We only analyzed the trials with saccades directed to the preferred location. Trials of each task were either randomly interleaved (6 total included sessions across both monkeys) or presented in blocks (14 sessions across both monkeys).

Neural recordings in the SC were performed with a 16- or 24-channel linear microelectrode array (AlphaOmega Inc., or Plexon, Inc., respectively) lowered hydraulically in the SC to record neural activity. The probe trajectory was approximately orthogonal to the SC and thus traversed its dorsoventral axis. Neural activity was recorded via the Grapevine Scout Neural Interface Processor (Ripple, Inc.), visualized with associated Trellis software, and communicated with our central data acquisition system. Neural activity was band-pass filtered between 250 Hz and 5 kHz to record spiking activity. Spike times were determined using a standard threshold. Spike trains and spike density waveforms were inspected online for task-related activity characteristic of the SC when a target was presented near the center of the response field. We will refer to the activity recorded across these contacts as each session's neural population. We also interleaved trials in which the target was placed at the diametrically opposite location, but those data are not considered here.

All analyses were performed using custom code written in MATLAB (MathWorks, Inc.). Saccades were detected using a 30 to 50°/s velocity criterion. For visualization purposes, we convolved the spike train with a Gaussian kernel of 10 ms width to yield spike density waveforms. For each session, we analyzed offline each channel's waveforms on a trial-by-trial and trial-averaged basis to ensure that each analyzed session consists of distinctive collicular activity across most channels for both the delay (10, 22) and gap tasks. To ensure that our results were not influenced by noise arising from too few trials, we set a criterion in which each session needed to have at least 30 trials from each task to be included. In most cases, each task condition had around 100 associated trials. Twenty (of 28) recording sessions met the above criteria (13 from monkey SU and 7 from BL) and comprise the dataset presented in this paper.

For each session, spiking activity from each channel was sorted into single units using MKsort, a supervised spike sorting interface (Ripple, Inc.). We found that both multiunit and single-unit populations resulted in similar population activity patterns after dimensionality reduction, which is in line with a recent study (62). From the 20 sessions presented in the paper, we recorded a total of 295 neurons (ranging from 7 to 26 neurons on a given session). All results, except for those in Fig. 1, were obtained from spike-sorted neural populations.

Data Analysis.

Definitions of sensory- and motor-related activity. We describe sensation and action epochs as the respective times at which the neural population responds most strongly to a visual stimulus and contributes to movement generation in each task. For the delay task, we found through visual inspection of target onset-aligned, trial-averaged activity that the visual burst peak time occurred approximately 160 ms after target appearance for most neurons and sessions. Thus, we used this static time for all analyses of the visual epoch. The motor burst typically peaked around the time of saccade onset; thus, we used saccade onset time as the epoch from which we extracted motor activity. For the gap task, we found that the visual burst peak tended to occur slightly earlier, at approximately 140 ms following stimulus onset, and thus was used as the visual epoch for this task. As in the delay task, motor activity was taken from saccade onset in each gap task trial. Sensory-related activity is represented with (light/dark) brown and motor-related activity with (light/dark) blue (e.g., Fig. 1*B*). These colors are used throughout the rest of our analyses comparing the neural activity underlying these key events.

Correlations across neurons. We analyzed the covariaiblity across neurons recorded simultaneously for individual sessions. In every session, we found the peak firing rate of each neuron at the desired epoch (visual or motor) for every trial in both the delay and gap tasks. After z-scoring the firing rates, we correlated firing rates across trials for all pairs of simultaneously recorded neurons in each recording session. A paired *t* test was performed for each individual session to determine whether the correlations were significantly different between tasks.

A correlation measure (Pearson) was then performed on the *P* values found from individual sessions and the classification accuracies found via LDA (*SI Appendix*, Fig. S5 *D–F*). Note that this analysis is not identical to noise correlation analyses (57) as our analysis only regards one time point in the trial (i.e., the timing of the visual or motor burst).

Features participating in high decoding performance. Following Nogueira et al. (29), we calculated how the separability of visual or motor activity patterns across tasks depends on fluctuations of various statistical features: PS, projected precision (PP), MPCs, and GA. Nogueira et al. assumed that the two covariance matrices (one for each task) were equivalent and used the average in their computations. Our data do not conform to this assumption (data not shown), but, nonetheless, we ignored this violation. To reliably compute the covariance matrices needed to calculate PP, we ensured that the number of trials for each task condition was 10 times the number of neurons recorded for that dataset (e.g., if 15 neurons were recorded simultaneously in one session, we required at least 150 trials for each of the two tasks). This restriction enabled us to perform this analysis on 9 datasets. For each session, we performed 1,000 bootstrapping iterations (subsample 40 trials with replacement). Next, we conditioned for one of the four statistical features. To do so, we selected the bootstrap values such that the other three statistical values were ±15th percentile around the median value (*SI Appendix*, Fig. S6). We calculated the percent change in decoding performance (DP% change) by first splitting the selected DP values into two groups: above and below the mean. Then, we found the difference between the groups and divided by the half below the mean. This process was repeated conditioning for each statistical feature of the neural activity from the visual and motor epochs across tasks (Fig. 6). We performed a one-tailed Wilcoxon signed-rank test to determine whether the DP% change was significantly greater than 0, as well as a Wilcoxon signed-rank test to determine whether the distributions were significantly different from one another.

Following Leavitt et al. (30), we removed the untuned neurons of each population and replicated our LDA analyses to see whether the contribution of untuned neurons significantly impacts the classification accuracies. For each dataset, a two-sample Kolmogorov–Smirnov test was performed to determine whether the firing rate distributions of a given neuron from each task were significantly different during either the visual or motor burst. If the distributions were not significantly different, the neuron was classified as untuned and removed from the analysis.

Dimensionality reduction. Dimensionality reduction methods are often used to summarize the population activity of simultaneously recorded neurons. They effectively reduce the number of dimensions by extracting redundancy and covariability across the neurons, and they transform the data into another reference frame. This approach also offers better visualization of neural activity and comparison across tasks (24).

FA is a dimensionality reduction algorithm that finds "latent factors" to explain the observed data. An individual's intelligence is an intuitive example of a latent factor. Intelligence by itself is an unobservable variable, but it explains correlated measurable variables such as test scores, GPA, and IQ. In the case of neural data analyses, FA finds latent factors that explain a neural population's spiking activity, taking into account both firing rates and higher-order statistics of the activities. The computation underlying FA can be thought of as a weighted linear summation that seeks to maximize the variance in spiking activity across neurons. The fundamental equation summarizing FA can be written as the following:

$$[\mathrm{Y}]_{n\times T} = \begin{bmatrix} b_{1,1} & \cdots & b_{1,m} \\ \vdots & \ddots & \vdots \\ b_{n,1} & \cdots & b_{n,m} \end{bmatrix}_{n\times m} [\mathrm{F}]_{m\times T} + [u]_{n\times T}, \qquad [\mathbf{1}]$$

where matrix Y is the observed spike trains of n simultaneously recorded neurons. Data from all neurons can be appended together in the formulation such that the number of columns T equals sum of the lengths of all trials used in the computation. The matrix F denotes the latent factors that are weighted to explain the commonalities among the observed neural data. The matrix u denotes the error terms or variance in Y that is unexplained by F. The $n \times m$ matrix consists of loading weights, with $b_{i,j}$ corresponding to the weight neuron i contributes to latent factor j. Neurons that contribute more to the overall variance across neurons will have higher weights and thus will have a larger influence in the weighted linear summation. The latent factors, F, are ranked according to the amount of shared variance accounted for. The first factor will capture the most variance across the population, the second will capture the second most, and so forth. Therefore, only a few dimensions are typically needed to capture a large portion of the variance found in the high-dimensional data, thereby reducing the dimensionality ($m < n$) needed to summarize the data.

We used a version of FA called GPFA. In addition to extracting a reduced number of latent factors that account for a large proportion of the variance, GPFA also simultaneously performs temporal smoothing, providing a more appealing visual representation of how activity evolves over time. We applied the GPFA algorithm in DataHigh, a publicly available MATLAB code (63), in which the input is formatted as a single structure that incorporates data from all trials across both tasks.

The input into the GPFA algorithm consists of a structure of the form

$$\left\{ \begin{bmatrix} n \times \dfrac{T_1}{\text{bin width}} \end{bmatrix} \\ \vdots \\ \begin{bmatrix} n \times \dfrac{T_s}{\text{bin width}} \end{bmatrix} \right\}_{S\times 1}, \qquad [\mathbf{2}]$$

where there is a total of S matrices, one for each trial. T represents the number of time points in a trial. As each trial has varying duration, the length of T varies across trials. The number of values for each trial is the original trial length divided by the bin width chosen by the user. We chose a bin width of 20 ms, and the value in each bin is the total number of spikes observed during the bin width period (64). The number of neurons, n, is consistent across trials. The output of GPFA consists of two variables: 1) the weighting matrix and 2) the reduced data. The weighting matrix consists of the projection weights found for every neuron in combination with each factor and takes the form shown in Eq. **1**. The maximum number of factors output by GPFA is equivalent to the number of neurons, so the weight matrix is $n \times m$ where $n = m$. The reduced data or "latent activity" is a structure resembling the input, where m remains equal to n:

$$\left\{ \begin{bmatrix} m \times \dfrac{T_1}{\text{bin width}} \end{bmatrix} \\ \vdots \\ \begin{bmatrix} m \times \dfrac{T_i}{\text{bin width}} \end{bmatrix} \right\}_{S\times 1}. \qquad [\mathbf{3}]$$

Importantly, however, these values are no longer high dimensional spiking data from each neuron but are now the reduced-dimensional, latent quantities. In other words, one latent factor does not correspond to one neuron, but rather to a weighted linear summation of all neurons' activities. We can then choose $m < n$ latent factors that account for sufficiently large percentage of the variance. Unless noted otherwise (e.g., *SI Appendix*, Fig. S2), we chose $m = 3$. A justification is provided in *Results*.

For the delay task, we treated activity from 200 ms before target onset to 200 ms after saccade onset on each task repetition as a full trial. For the gap task, a full trial was considered to start 200 ms before target onset and end 600 ms after target onset (which includes the period of time in which a saccade is made). The GPFA algorithm does not have knowledge of the task to which a given trial belongs; only the user has this information. Thus, when GPFA maximizes the variance across neural activity, it uses the activity from all trials regardless of context. Only when plotting this latent activity do we identify which task type each point comes from, via color, to determine whether patterns are distinct depending on context.

When initially plotting state-space activity for each session, we observed that a few sessions ($N = 3$) had a subspace shift within either the delay or gap task for a subset of trials. When plotting the latent activity values against trial number, we saw for these sessions an abrupt trial on which the subspace shifted, potentially indicative of an electrode shift or the addition/loss of signal on one channel. For these sessions, we retained only the subset of trials for which the delay and gap task subspaces remained constant, discarding trials before or after the shift.

In a separate analysis, we performed GPFA on delay task trials only and then projected gap task trials into the same low-dimensional space. In this case, the weighting matrix is calculated using only delay task data rather than data

from both tasks. The latent activity for the gap task is then found by using the weights calculated using only the delay data. Thus, the gap activity is "projected" into the same latent, low-dimensional space as the delay task, contrasting our main method of determining latent factors using both delay and gap data. This approach yielded qualitatively similar subspaces (not shown). We also compared subspaces using matched visual burst times for both tasks (140 ms after target onset) and found them to be qualitatively similar to those formed by activity at the estimated visual burst peak time for each task (160 ms for delay; 140 ms for gap), indicating that our analyses of population activity patterns are not highly sensitive to the chosen event time during the visual epoch.

LDA classification. A two-class linear classifier (LDA) was implemented to determine the amount of separability between various pairs of subspaces in the low-dimensional state space found via GPFA. We trained the classifier using a random partition of 70% of the data and the assigned class labels. The classifier was then tested on the remaining data points (60, 65). For the analysis reported in Fig. 3, we trained and tested the classifier on data partitioned and labeled as visual and motor for each trial type. For Fig. 4, we trained and tested the classifier on data partitioned and labeled as delay and gap for each epoch. In Fig. 5 *A* and *C*, we trained and tested the classifier to discriminate between visual and motor epochs when data from both tasks were combined. In Fig. 5 *B* and *E*, we trained and tested the classifier to discriminate between delay and gap tasks when data from both epochs were pooled together. LDA defines a decision boundary, or hyperplane, that maximizes the separability between the two classes. Classification accuracies were found by determining the number of instances in which the classifier accurately identified a point associated with a given label and then dividing by the total number of data points that should have been classified as such. To confirm the statistical significance of these results, we performed 100 iterations of LDA on each data session. Presented in the results are the average classification accuracies taken across the 100 iterations for each data session. In addition, a control analysis was performed in which the categorical labels were randomly shuffled before the classifier was implemented to confirm our chance level was near the expected 50%. The orthogonality between the LDA planes separating visual and motor activity and delay and gap activity was determined by finding the angle between the two vectors normal to each plane. This angle was calculated by taking the arccosine of the normalized dot product of these vectors.

A paired Wilcoxon signed-rank test was performed on the two distributions of classification accuracy values in Figs. 3 and 4 to determine whether the median difference between the two paired distributions was different from zero at an $\alpha = 0.05$ significance level. Additionally, a one-tailed Wilcoxon signed-rank test was performed on each individual distribution in Figs. 3–5 and *SI Appendix*, Figs. S3 and S4 to determine whether the median classification accuracy was significantly above the chance level of the classifier. Last, for each individual session, we performed a *t* test on the distribution of behavioral characteristics from the delay and gap conditions, as depicted in *SI Appendix*, Fig. S1*A* (saccade peak velocity) and 1B (saccade amplitude), followed by a *t* test on the distribution of trial-averaged values from each condition across all sessions.

Comparison of pooled single-unit activity with our targeted population-level approach. For both the delay and gap tasks, peak firing rates in each epoch (visual and motor) were compared to determine whether pooled activity from all recorded neurons could be readily differentiated across tasks via firing rate differences alone (Fig. 1 *C* and *D*). For each included session (N = 20), each neuron had to satisfy a 30 spikes per second threshold in any epoch of either task to be used for comparison. A paired *t* test was then performed for each individual session as well as all sessions pooled to determine whether firing rates were significantly different between tasks. A correlation measure (Pearson) was then performed on the *P* values found from individual sessions and the classification accuracies found via LDA (*SI Appendix*, Fig. S5).

Data, Materials, and Software Availability. Data in MATLAB form are available at https://github.com/ecayar/Gap_Task_Project_GandhiLab.git (66). Custom MATLAB code used for this study is available at https://github.com/ecayar/Gap_Task_Project_GandhiLab.git (66).

ACKNOWLEDGMENTS. Portions of the paper were developed from the doctoral dissertation of M.R.H. This work was supported by NIH Grants R01 EY024831 and R01 EY022854 to N.J.G., R90 DA023426 to E.C.A., and Achievement Rewards for College Students Foundation Award and Graduate Assistance in Areas of National Need Fellowship (P200A150050) to M.R.H. We would like to thank Dr. Corentin Massot for assistance with data collection and Dr. Ramon Nogueira for discussions regarding their data analysis.

Author affiliations: [a]Department of Neuroscience, University of Pittsburgh, Pittsburgh, PA 15213; [b]Program in Neural Computation, Carnegie Mellon University, Pittsburgh, PA 15213; [c]Center for Neural Basis of Cognition, University of Pittsburgh, Pittsburgh, PA 15213; [d]Department of Bioengineering, University of Pittsburgh, Pittsburgh, PA 15213; and [e]Center for Neuroscience, University of Pittsburgh, Pittsburgh, PA 15213

1. B. Reuter, N. Kathmann, Using saccade tasks as a tool to analyze executive dysfunctions in schizophrenia. *Acta Psychol. (Amst)* **115**, 255–269 (2004).
2. S. B. Hutton, Cognitive control of saccadic eye movements. *Brain Cogn.* **68**, 327–340 (2008).
3. U. K. Jagadisan, N. J. Gandhi, Disruption of fixation reveals latent sensorimotor processes in the superior colliculus. *J. Neurosci.* **36**, 6129–6140 (2016).
4. M. G. Saslow, Latency for saccadic eye movement. *J. Opt. Soc. Am.* **57**, 1030–1033 (1967).
5. M. C. Dorris, D. P. Munoz, A neural correlate for the gap effect on saccadic reaction times in monkey. *J. Neurophysiol.* **73**, 2558–2562 (1995).
6. D. Sparks, W. H. Rohrer, Y. Zhang, The role of the superior colliculus in saccade initiation: A study of express saccades and the gap effect. *Vision Res.* **40**, 2763–2777 (2000).
7. R. H. Wurtz, M. A. Sommer, M. Paré, S. Ferraina, Signal transformations from cerebral cortex to superior colliculus for the generation of saccades. *Vision Res.* **41**, 3399–3412 (2001).
8. N. J. Gandhi, H. A. Katnani, Motor functions of the superior colliculus. *Annu. Rev. Neurosci.* **34**, 205–231 (2011).
9. M. A. Basso, P. J. May, Circuits for action and cognition: A view from the superior colliculus. *Annu. Rev. Vis. Sci.* **3**, 197–226 (2017).
10. C. Massot, U. K. Jagadisan, N. J. Gandhi, Sensorimotor transformation elicits systematic patterns of activity along the dorsoventral extent of the superior colliculus in the macaque monkey. *Commun. Biol.* **2**, 287 (2019).
11. D. P. Munoz, R. H. Wurtz, Saccade-related activity in monkey superior colliculus. II. Spread of activity during saccades. *J. Neurophysiol.* **73**, 2334–2348 (1995).
12. M. C. Dorris, D. P. Munoz, Saccadic probability influences motor preparation signals and time to saccadic initiation. *J. Neurosci.* **18**, 7015–7026 (1998).
13. R. A. Marino *et al.*, Linking visual response properties in the superior colliculus to saccade behavior. *Eur. J. Neurosci.* **35**, 1738–1752 (2012).
14. R. A. Marino, R. Levy, D. P. Munoz, Linking express saccade occurance to stimulus properties and sensorimotor integration in the superior colliculus. *J. Neurophysiol.* **114**, 879–892 (2015).
15. R. A. Marino, R. Levy, D. P. Munoz, Distinct sensory- and goal-related signals underlie the gap effect in the superior colliculus. *Eur. J. Neurosci.* **55**, 205–226 (2022).
16. M. C. Dorris, M. Paré, D. P. Munoz, Neuronal activity in monkey superior colliculus related to the initiation of saccadic eye movements. *J. Neurosci.* **17**, 8566–8579 (1997).
17. J. A. Edelman, M. E. Goldberg, Dependence of saccade-related activity in the primate superior colliculus on visual target presence. *J. Neurophysiol.* **86**, 676–691 (2001).
18. M. M. Churchland *et al.*, Stimulus onset quenches neural variability: A widespread cortical phenomenon. *Nat. Neurosci.* **13**, 369–378 (2010).
19. M. T. Kaufman, M. M. Churchland, S. I. Ryu, K. V. Shenoy, Cortical activity in the null space: Permitting preparation without movement. *Nat. Neurosci.* **17**, 440–448 (2014).
20. G. F. Elsayed, A. H. Lara, M. T. Kaufman, M. M. Churchland, J. P. Cunningham, Reorganization between preparatory and movement population responses in motor cortex. *Nat. Commun.* **7**, 13239 (2016).
21. A. H. Lara, J. P. Cunningham, M. M. Churchland, Different population dynamics in the supplementary motor area and motor cortex during reaching. *Nat. Commun.* **9**, 2754 (2018).
22. U. K. Jagadisan, N. J. Gandhi, Population temporal structure supplements the rate code during sensorimotor transformations. *Curr. Biol.* **32**, 1010–1025.e9 (2022).
23. C. Bourrelly, C. Massot, N. J. Gandhi, Rapid input-output transformation between local field potential and spiking activity during sensation but not action in the superior colliculus. *J. Neurosci.* **43**, 4047–4061 (2023).
24. J. P. Cunningham, B. M. Yu, Dimensionality reduction for large-scale neural recordings. *Nat. Neurosci.* **17**, 1500–1509 (2014).
25. M. R. Heusser, U. K. Jagadisan, N. J. Gandhi, Drifting representation with transient resets characterizes sensorimotor transformation in the monkey superior colliculus. bioRxiv [Preprint] (2023). https://doi.org/10.1101/2023.01.03.522634 (Accessed 1 September 2023).
26. E. Zohary, M. N. Shadlen, W. T. Newsome, Correlated neuronal discharge rate and its implications for psychophysical performance. *Nature* **370**, 140–143 (1994).
27. A. S. Ecker *et al.*, Decorrelated neuronal firing in cortical microcircuits. *Science* **327**, 584–587 (2010).
28. I. C. Lin, M. Okun, M. Carandini, K. D. Harris, The nature of shared cortical variability. *Neuron* **87**, 644–656 (2015).
29. R. Nogueira *et al.*, The effects of population tuning and trial-by-trial variability on information encoding and behavior. *J. Neurosci.* **40**, 1066–1083 (2020).
30. M. L. Leavitt, F. Pieper, A. J. Sachs, J. C. Martinez-Trujillo, Correlated variability modifies working memory fidelity in primate prefrontal neuronal ensembles. *Proc. Natl. Acad. Sci. U.S.A.* **114**, E2494–E2503 (2017).
31. R. J. Krauzlis, L. P. Lovejoy, A. Zénon, Superior colliculus and visual spatial attention. *Annu. Rev. Neurosci.* **36**, 165–182 (2013).
32. B. Cooper, R. M. McPeek, Role of the superior colliculus in guiding movements not made by the eyes. *Annu. Rev. Vis. Sci.* **7**, 279–300 (2021).

33. V. E. Das, Strabismus and the oculomotor system: Insights from macaque models. *Annu. Rev. Vis. Sci.* **2**, 37–59 (2016).
34. D. L. Sparks, Conceptual issues related to the role of the superior colliculus in the control of gaze. *Curr. Opin. Neurobiol.* **9**, 698–707 (1999).
35. L. P. Lovejoy, R. J. Krauzlis, Inactivation of primate superior colliculus impairs covert selection of signals for perceptual judgments. *Nat. Neurosci.* **13**, 261–266 (2010).
36. S. Everling, M. C. Dorris, R. M. Klein, D. P. Munoz, Role of primate superior colliculus in preparation and execution of anti-saccades and pro-saccades. *J. Neurosci.* **19**, 2740–2754 (1999).
37. U. K. Jagadisan, N. J. Gandhi, Removal of inhibition uncovers latent movement potential during preparation. *Elife* **6**, e29648 (2017).
38. K. A. Dyckman, J. Camchong, B. A. Clementz, J. E. McDowell, An effect of context on saccade-related behavior and brain activity. *Neuroimage* **36**, 774–784 (2007).
39. E. L. Keller, K. M. Lee, R. M. McPeek, Readout of higher-level processing in the discharge of superior colliculus neurons. *Ann. N. Y. Acad. Sci.* **1039**, 198–208 (2005).
40. T. B. Crapse, H. Lau, M. A. Basso, A role for the superior colliculus in decision criteria. *Neuron* **97**, 181–194.e6 (2018).
41. R. M. McPeek, E. L. Keller, Saccade target selection in the superior colliculus during a visual search task. *J. Neurophysiol.* **88**, 2019–2034 (2002).
42. K. Shen, J. Valero, G. S. Day, M. Paré, Investigating the role of the superior colliculus in active vision with the visual search paradigm. *Eur. J. Neurosci.* **33**, 2003–2016 (2011).
43. T. Ikeda, O. Hikosaka, Positive and negative modulation of motor response in primate superior colliculus by reward expectation. *J. Neurophysiol.* **98**, 3163–3170 (2007).
44. M. F. Walker, E. J. Fitzgibbon, M. E. Goldberg, Neurons in the monkey superior colliculus predict the visual result of impending saccadic eye movements. *J. Neurophysiol.* **73**, 1988–2003 (1995).
45. C. A. Dunn, N. J. Hall, C. L. Colby, Spatial updating in monkey superior colliculus in the absence of the forebrain commissures: Dissociation between superficial and intermediate layers. *J. Neurophysiol.* **104**, 1267–1285 (2010).
46. T. R. Darlington, S. G. Lisberger, Mechanisms that allow cortical preparatory activity without inappropriate movement. *Elife* **9**, e50962 (2020).
47. T. Ikeda *et al.*, Spatio-temporal response properties of local field potentials in the primate superior colliculus. *Eur. J. Neurosci.* **41**, 856–865 (2015).
48. C. W. Mohler, R. H. Wurtz, Organization of monkey superior colliculus: Intermediate layer cells discharging before eye movements. *J. Neurophysiol.* **39**, 722–744 (1976).
49. A. Afshar *et al.*, Single-trial neural correlates of arm movement preparation. *Neuron* **71**, 555–564 (2011).
50. L. Duncker, M. Sahani, Dynamics on the manifold: Identifying computational dynamical activity from neural population recordings. *Curr. Opin. Neurobiol.* **70**, 163–170 (2021).
51. J. A. Edelman, E. L. Keller, Activity of visuomotor burst neurons in the superior colliculus accompanying express saccades. *J. Neurophysiol.* **76**, 908–926 (1996).
52. K. Kim, C. Lee, Activity of primate V1 neurons during the gap saccade task. *J. Neurophysiol.* **118**, 1361–1375 (2017).
53. J. Lee, J. M. Groh, Different stimuli, different spatial codes: A visual map and an auditory rate code for oculomotor space in the primate superior colliculus. *PLoS One* **9**, e85017 (2014).
54. T. Zhang, T. Malevich, M. P. Baumann, Z. M. Hafed, Superior colliculus saccade motor bursts do not dictate movement kinematics. *Commun. Biol.* **5**, 1222 (2022).
55. M. P. Baumann, A. R. Bogadhi, A. F. Denninger, Z. M. Hafed, Sensory tuning in neuronal movement commands. bioRxiv [Preprint] (2022). https://doi.org/10.1101/2022.11.08.515621 (Accessed 1 September 2023).
56. L. N. Katz, G. Yu, J. P. Herman, R. J. Krauzlis, Correlated variability in primate superior colliculus depends on functional class. *Commun. Biol.* **6**, 540 (2023).
57. M. R. Cohen, A. Kohn, Measuring and interpreting neuronal correlations. *Nat. Neurosci.* **14**, 811–819 (2011).
58. S. B. Khanna, A. C. Snyder, M. A. Smith, Distinct sources of variability affect eye movement preparation. *J. Neurosci.* **39**, 4511–4526 (2019).
59. A. H. Lara, G. F. Elsayed, A. J. Zimnik, J. P. Cunningham, M. M. Churchland, Conservation of preparatory neural events in monkey motor cortex regardless of how movement is initiated. *Elife* **7**, e31826 (2018).
60. M. R. Heusser, C. Bourrelly, N. J. Gandhi, Decoding the time course of spatial information from spiking and local field potential activities in the superior colliculus. *eNeuro* **9**, ENEURO.0347-0322.2022 (2022).
61. C. L. Bryant, N. J. Gandhi, Real-time data acquisition and control system for the measurement of motor and neural data. *J. Neurosci. Methods* **142**, 193–200 (2005).
62. E. M. Trautmann *et al.*, Accurate estimation of neural population dynamics without spike sorting. *Neuron* **103**, 292–308.e4 (2019).
63. B. R. Cowley *et al.*, DataHigh: Graphical user interface for visualizing and interacting with high-dimensional neural activity. *J. Neural. Eng.* **10**, 066012 (2013).
64. B. M. Yu *et al.*, Gaussian-process factor analysis for low-dimensional single-trial analysis of neural population activity. *J. Neurophysiol.* **102**, 614–635 (2009).
65. I. Smalianchuk, N. J. Gandhi, Ventral premotor cortex encodes task relevant features during eye and head movements. *Sci. Rep.* **12**, 22093 (2022).
66. E. C. Ayar, Gap_Task_Project_GandhiLab. Github. https://github.com/ecayar/Gap_Task_Project_GandhiLab. Accessed 1 September 2023.